Research Article

ADVANCED PHOTONICS

Spatiotemporal topology of plasmonic spin meron pairs revealed by polarimetric photo-emission microscopy

Pascal Dreher,[a,†] Alexander Neuhaus,[a,†] David Janoschka,[a,†] Alexandra Rödl,[a] Tim Colin Meiler,[b] Bettina Frank,[b] Timothy J. Davis,[a,b,c,*] Harald Giessen,[b,*] and Frank Meyer zu Heringdorf[a,*]

[a]University of Duisburg-Essen, Faculty of Physics and CENIDE, Duisburg-Essen, Duisburg, Germany
[b]University of Stuttgart, 4th Physics Institute and Research Center SCoPE, Stuttgart, Germany
[c]University of Melbourne, School of Physics, Parkville, Victoria, Australia

Abstract. Topology is the study of geometrical properties and spatial relations unaffected by continuous changes and has become an important tool for understanding complex physical systems. Although recent optical experiments have inferred the existence of vector fields with the topologies of merons, the inability to extract the full three-dimensional vectors misses a richer set of topologies that have not yet been fully explored. We extend the study of the topology of electromagnetic fields on surfaces to a spin quasi-particle with the topology of a meron pair, formed by interfering surface plasmon polaritons (SPPs), and show that the in-plane vectors are constrained by the embedding topology of the space as dictated by the Poincaré–Hopf theorem. In addition, we explore the time evolution of the three-dimensional topology of the spin field formed by femtosecond laser pulses. These experiments are possible using our here-developed method called polarimetric photo-emission electron microscopy (polarimetric PEEM), which combines an optical pump–probe technique and polarimetry with PEEM. This method allows for the accurate generation of SPP fields and their subsequent measurement, revealing both the spatial distribution of the full three-dimensional electromagnetic fields at deep subwavelength resolution and their time evolution.

Keywords: spin; photonics; electron microscopy; plasmonics; topology; ultrafast optics.

Received Nov. 19, 2024; accepted for publication Nov. 22, 2024; published online Dec. 16, 2024.

[DOI: 10.1117/1.AP.6.6.066007]

1 Introduction

The topology of spin states in matter has a profound influence on material properties, underpinning the robustness of solid-state systems such as those exhibiting the quantum Hall effect.[1] The topology imposes constraints on the physical parameters that stabilize these systems, as with the magnetic spins in thin films, where stable configurations often have the topology of a skyrmion.[2,3] Such vortex-like topological solitons are robust to thermal fluctuations, due to the Dzyaloshinskii–Moriya interaction, which creates an energy barrier against breaking the topology. Their stability and small size hold promise for their use in information storage.[4] Likewise, the half skyrmion, or meron, is an important topological feature in magnetic films, where the magnetic spin vectors can be mapped onto a hemisphere. Merons are also of interest for applications in magnetic memories,[5] but unlike skyrmions, merons on continuous films are not energetically stable and cannot exist in isolation.[6,7] In these films, merons tend to form in pairs, but their formation in magnetic thin films is difficult to achieve, and evidence for their existence has been inferred only in structured magnetic films.[7–10]

In contrast to magnetic films, photonic systems provide a convenient paradigm for generating and studying vector fields with different topologies. Topological vortices associated with the vector nature of optical fields have been demonstrated in recent experiments,[11] but only a few have had the topology of a meron. Meron spin structures were generated in the mode

*Address all correspondence to Timothy J. Davis, timd@unimelb.edu.au; Harald Giessen, h.giessen@pi4.uni-stuttgart.de; Frank Meyer zu Heringdorf, meyerzh@uni-due.de

†These authors contributed equally to this work.

structure of an optical cavity filled with liquid crystal,[12] with the topology of a bimeron, and have been observed in phonon–polariton fields.[13] Merons also appear in the spin textures of interfering surface plasmon polaritons (SPPs). A trimeron spin structure[14] and a meron spin lattice[15] were inferred from measures of the in-plane electric field distributions in time-resolved photo-emission electron microscopy (PEEM). Despite these experimental demonstrations, there has been no complete measure of the spin fields of optical merons and the subsequent direct measure of their topology. Unlike magnetic films, features in the electromagnetic fields of optical systems generally have no energy barriers associated with their topology because they are formed by interfering waves. Nevertheless, as we discuss below, there are constraints imposed by the field topology that can be revealed in their spin textures.

In this work, we investigate experimentally the topology of a meron pair that we create by interfering SPPs on the surface of a gold crystal. The merons appear as a pair of spin quasiparticles arising from the rotations of the SPP electric and magnetic fields. These complex spin textures depend on the spatiotemporal properties of both the electric and magnetic fields and are thus difficult to access experimentally. We show that such complex spin textures in the SPP fields can be measured and characterized on the deep subwavelength scale with subfemtosecond accuracy using a new technique that we call polarimetric PEEM, which utilizes multiple distinct polarizations of the probe laser field to unambiguously extract the vector components of the meron's electric field. From our experimental measurements, we compute the Chern number that classifies the topology. We begin with a brief discussion of the topology of merons and then detail the experimental system that enables us to excite and measure the SPP electric field and to extract the complete magnetic field and spin distribution in space and time. With this information, we explore the complete topology of the meron pair and show that the in-plane vectors obey the Poincaré–Hopf theorem, which links differential geometry to topology and provides a global topological constraint on the in-plane spin vectors.

2 Methods

The experiments to determine the topology of the SPP spin merons were performed using a spectroscopic photo-emission and low-energy electron microscope (ELMITEC SPE-LEEM III) equipped with a TVIPS F216 detector.[16] Optical excitation and probing of SPPs were performed using a Ti:sapphire laser oscillator (FEMTOLASERS). The laser system generates 15 fs short pulses at a central wavelength of 800 nm and at a repetition rate of 80 MHz. The pulses are guided through the electron-optical setup of the SPE-LEEM and impinge under normal incidence.[17] For the time-resolved experiments, an actively phase-stabilized Mach–Zehnder interferometer with polarization control was used [see Supplementary Material (Note 1) for details]. All polarization states were controlled using retarding wave plates, and each polarization was verified using a commercial optical polarimeter. Samples were fabricated *ex-situ* by a single-step thermolysis of ($AuCl_4$)-tetraoctylammonium bromide on a native SiO_2 layer on a Si substrate.[18] A focused ion beam (Raith ionLINE Plus) was used to mill grooves into the resulting Au(111) crystals. The grooves provide momentum matching and enable the conversion of the laser pulses into SPPs at defined positions. After transfer to the SPE-LEEM, the samples were cleaned by standard Ar sputtering and annealing, and the work function of the Au was lowered by deposition of a submonolayer of Cs. Details of the data analysis are described in Supplementary Material (Notes 2 and 3).

3 Results and Discussion

The topology of a vector field is classified by the Chern number C, which describes the number of times the vectors map over the surface of a sphere.[19,20] For a distribution of spin vectors $\mathbf{s}$ over the x–y plane, the Chern number is obtained from a surface integral over the Chern density involving the unit spin vectors $\hat{\mathbf{s}}$:

$$C = \frac{1}{4\pi}\int_A \hat{\mathbf{s}} \cdot (\partial_x \hat{\mathbf{s}} \times \partial_y \hat{\mathbf{s}}) \mathrm{d}A. \tag{1}$$

With this classification, skyrmions are vector fields with a Chern number of $C = 1$, whereas merons have a Chern number of $C = 1/2$, which constrains the distributions of the vector fields in three dimensions. Less well known is that the projections of vector fields onto the surface, as associated with SPPs, are also constrained by the two-dimensional topology of the space and the distributions of the vectors on the boundary. This constraint arises from the Poincaré–Hopf theorem,[21,22] which relates the differential geometry of the vector field to the topology of the space in which it is embedded, as represented by the Euler characteristic of the surface geometry, which is a topological invariant.

A spin texture with the topology of a meron can come in four different types related to the direction of the out-of-plane vector at its center and the direction of rotation of the in-plane vector fields about the central point, with examples shown in Fig. 1(a) (here the surface is taken as the x–y plane with the normal in the z direction). The point where all the in-plane spin vectors $s_x = s_y = 0$ are zero is known as a C point because the electric fields here are perfectly circularly polarized in the plane of the surface.[20,23,24] Accordingly, there is only an out-of-plane spin vector so that $s_z \neq 0$ here. The sign of this vector component determines a quantity called the polarity p. If the spin vector is positive $s_z > 0$, then the polarity of the meron is $p = 1/2$, and if the out-of-plane spin is negative, $s_z < 0$, then $p = -1/2$.[11,19] If one traverses a loop about this point in an anticlockwise direction [black-dotted line in Fig. 1(a)], the in-plane spin vectors (depicted as arrows) rotate either in a clockwise or anticlockwise sense. The direction of rotation of these vectors in space is known as the vorticity v, with $v = 1$ for anticlockwise rotation and $v = -1$ for clockwise rotation. With this characterization, the Chern number of a given isolated feature is the product[19] $C = p \cdot v$. This formula is based on the assumption that the feature has certain symmetry properties.[19] Associated with C points are L lines, which are lines of pure linear polarization of the in-plane electric fields. The L lines occur where the out-of-plane spin $s_z = 0$ and can be used to delineate the boundary of a local topological feature, as used in studying individual merons[14] and meron lattices.[15]

The two-dimensional representation of the vectors in Fig. 1(a) provides no information on the polarity of the spin, even though for this example we have arbitrarily set the polarities as shown. In principle, the sign of the polarity can be changed without affecting the vorticity. This degeneracy is a consequence of the reflection symmetry of the in-plane vectors s_x and s_y in the x–y plane, whereas s_z changes sign on reflection. As a consequence, we need to measure the complete vector

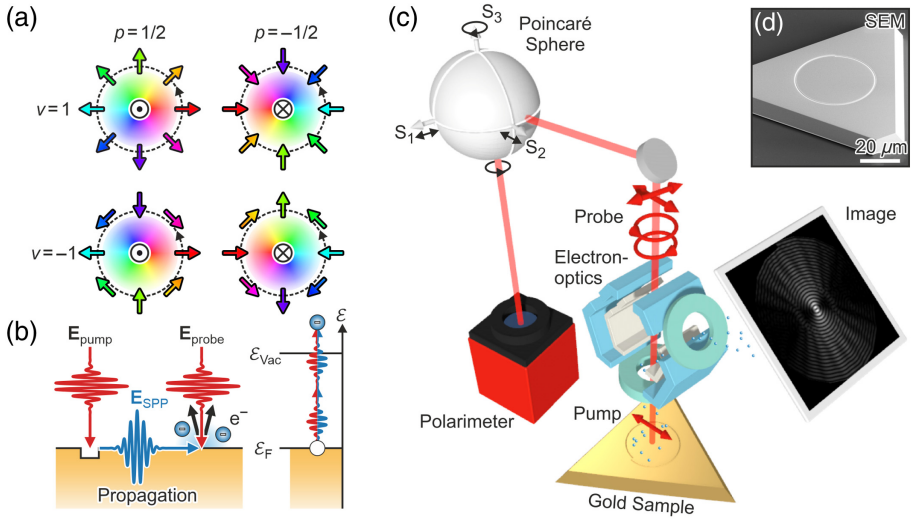

Fig. 1 Topology of a meron and the experimental arrangement used to measure the SPP spin texture. (a) Four possible configurations of spin for a meron, represented by (p, v), with polarity p and vorticity v. The color hue encodes the direction of the in-plane vectors, with example arrows drawn around the boundary (black dotted line). The circles represent the direction of the out-of-plane spin (dot $s_z > 0$, cross $s_z < 0$). The singularity at the center is where the in-plane vectors are zero; (b) the experimental procedure involves the excitation of the SPP by the optical pump beam, the propagation of the SPP over the surface, and the subsequent interference with a probe light beam, resulting in two-photon absorption and the emission of a photo-electron; (c) a schematic of the experimental arrangement; and (d) a scanning electron microscope image of a single Au crystal with an Archimedean spiral etched into its surface.

field to correctly determine both the polarity and vorticity. Accordingly, knowledge of the full three-dimensional spin vectors $\mathbf{s}(x, y)$ over the surface is required to characterize the topology of any SPP spin texture that we excite. We obtain this information using time-resolved PEEM based on a new optical pump–probe method that is a significant progression of the method we used to measure a skyrmion lattice created from SPP electric fields.[25]

3.1 Polarimetric PEEM

The SPP spin textures are generated and investigated in a pump–probe PEEM experiment with subfemtosecond accuracy. The SPP spin textures are formed by illuminating a grating coupler with a femtosecond (pump) laser pulse, and the subsequent measurement is achieved by imaging the photo-electron distribution emitted by a second (probe) laser pulse in the PEEM [Figs. 1(b) and 1(c)]. As such, the first illumination pulse excites the SPPs, and the second pulse probes the SPP vector field directions.[26] The PEEM detects photo-electrons that are liberated in a second-order photo-emission process resulting from the interfering SPP and probe electric fields[27] [Fig. 1(b)]. From data sequences created with different pump–probe time delays and different probe polarizations, we reconstruct the full spatiotemporal vectorial electric field, allowing us to reconstruct the spin field.

To excite SPPs with the desired topology, the linear polarization of the first (pump) pulse is configured with respect to grooves etched into a single-crystalline Au sample [Figs. 1(c) and 1(d)]. The grooves form an Archimedean spiral that increases in radius by one SPP wavelength λ_{spp} over 2π rad. See Supplementary Material (Note 4) for details on the shape of the groove and the relative orientation of the pump polarization. Once excited, the SPPs propagate over the surface of the metal and interfere at the center of the structure, where they form vortex quasi-particles with the topology of a meron pair. The normally incident second (probe) pulse arrives after a predetermined time delay and interferes with the in-plane components of the SPP fields created by the pump pulse [Fig. 1(b)]. The combined electric field leads to a second-order absorption process and the liberation of photo-electrons with an electron yield Y related to the square of the time-integrated intensity I,

$$Y \propto \int I^2 \mathrm{d}t \propto \int |E_{\mathrm{probe}}|^4 + |E_{\mathrm{spp}}|^4 + 2|E_{\mathrm{probe}}|^2|E_{\mathrm{spp}}|^2 + 4\,\mathrm{Re}(\mathbf{E}^*_{\mathrm{probe}} \cdot \mathbf{E}_{\mathrm{spp}})^2 + 4(|E_{\mathrm{probe}}|^2 + |E_{\mathrm{spp}}|^2)\mathrm{Re}(\mathbf{E}^*_{\mathrm{probe}} \cdot \mathbf{E}_{\mathrm{spp}})\mathrm{d}t, \quad (2)$$

with the probe and SPP electric fields given by $\mathbf{E}_{\mathrm{probe}}$ and $\mathbf{E}_{\mathrm{spp}}$, respectively. The integral accounts for the time integration by the electron detector of the PEEM. The last term in Eq. (2) yields information on the projection of the in-plane SPP electric field with the probe field via $\mathbf{E}^*_{\mathrm{probe}} \cdot \mathbf{E}_{\mathrm{spp}}$, and only this term contains the fundamental SPP wave vector $\mathbf{k}_{\mathrm{spp}}$ and the fundamental frequency ω [see Supplementary Material (Note 3) for a more detailed discussion of the scaling of the terms]. We isolate this term from the extraneous ones in Eq. (2) by performing a spatiotemporal Fourier decomposition of the photo-electron yield.[25,26] Repeating the experiment with different probe polarizations and extracting these signal components enables the full reconstruction of the SPP vector field. Examples of PEEM

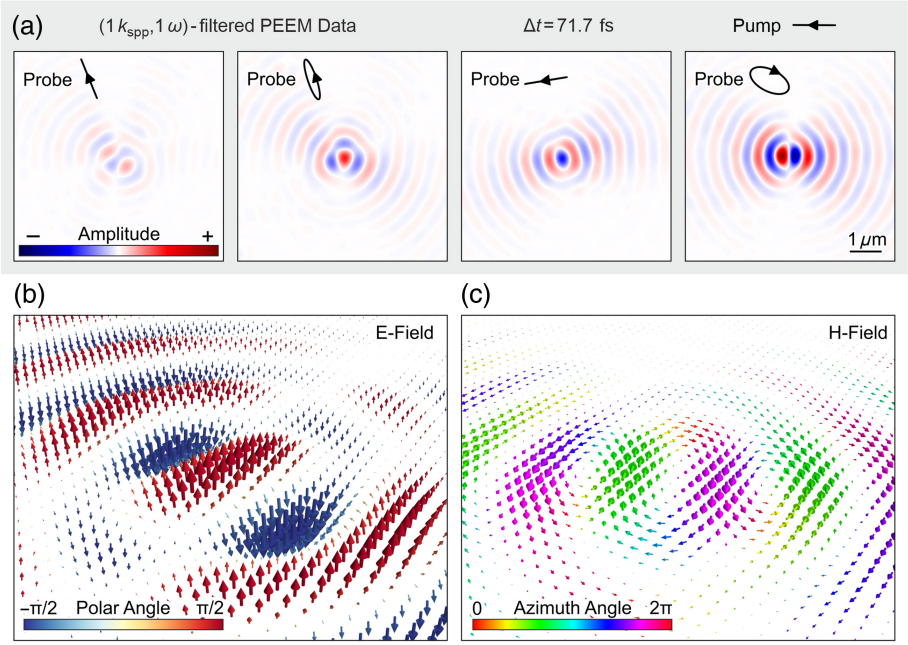

Fig. 2 Examples of the measured electric and magnetic fields from the polarimetric PEEM method. (a) The measured SPP electric field projections $\mathbf{E}^*_{\text{probe}} \cdot \mathbf{E}_{\text{spp}}$ after Fourier filtering for four different probe polarization states, at a pump–probe delay time of $\Delta t = 71.7$ fs; (b) a three-dimensional rendering of the SPP electric field (time-dependency shown in Video 1) obtained by combining the data in panel (a) and using the fact that the electric field divergence is zero; (c) a three-dimensional rendering of the derived magnetic field (time-dependency shown in Video 1) obtained from the electric field using Maxwell's equations. (Video 1, M4V, 16.2 MB [URL: https://doi.org/10.1117/1.AP.6.6.066007.s1]; Video 2, M4V, 21.6 MB [URL: https://doi.org/10.1117/1.AP.6.6.066007.s2].)

measurements after Fourier filtering for the four different probe polarizations are shown in Fig. 2(a).

There are four key issues with reconstructing the electric field vectors. First, the polarization of the probe pulse needs to be accurately measured, which is done before each experiment to determine the Stokes vectors that characterize the precise polarization. Moreover, we use four different polarization states (two linear and two elliptical) and apply a minimization procedure to combine the results to improve the measurement statistics. Second, the images from each measurement must be aligned to correct for the thermal drift of the sample in the PEEM vacuum chamber; otherwise, the field vectors cannot be accurately reconstructed. Third, identifying the time zero, when the pump and probe pulse overlap exactly, is necessary for all the probe pulses to correctly phase the different images to obtain accurate measures of the SPP field vectors and their time variation. This is achieved using a spectral interference method, described in Supplementary Material (Note 2). Finally, because of the difficulty in centering the focused pump beam on the sample in the PEEM vacuum chamber, the Archimedean spiral is not exactly uniformly illuminated, which results in additional terms to the SPP field measurement. However, these artifacts have an asymmetric spatial dependence that can be removed by symmetrizing the fields in the Fourier space. The field reconstruction is then performed by a fixed-point iteration, as discussed in detail in Supplementary Material (Note 3). The result of the reconstruction is a very clean measure of the SPP field $\mathbf{E}_{\text{spp}}(\mathbf{r}, t)$ as a function of position $\mathbf{r}$ over the sample surface and as a function of time t.

With this "polarimetric" PEEM technique, we obtain the time evolution of the SPP electric field $\mathbf{E}_{\text{spp}}(\mathbf{r}, t)e^{-i\omega t}$ that we write as the product of a phase, which oscillates at the central frequency ω of the light pulse, and a complex amplitude $\mathbf{E}_{\text{spp}}(\mathbf{r}, t)$ that varies in time according to the envelope of the laser pulse and the propagation of the SPP wave. The SPP electric field measured by this technique at a delay time of $\Delta t = 71.7$ fs is shown as a three-dimensional rendering in Fig. 2(b). Applying Maxwell's equations to this measured field, we compute the SPP magnetic field $\mathbf{H}_{\text{spp}}(\mathbf{r}, t)e^{-i\omega t}$ [Fig. 2(c)]. This field lies entirely in the x–y plane, which is the surface plane of the Au film. These fields are obtained at a maximal spatial resolution of ≈10 nm, which is the resolution of the PEEM, and with a delay-time-discretization of 0.16 fs. We benchmark our new technique in Supplementary Material (Note 5) by applying it to the trimeron spin texture that was previously investigated by Dai et al.[14]

3.2 Spin Textures

From the complete measurements of the spatial and temporal evolution of the SPP electromagnetic fields, we calculate the spin angular momentum density using

$$\mathbf{s}(\mathbf{r}, t) = \text{Im}(\varepsilon \mathbf{E}^*_{\text{spp}} \times \mathbf{E}_{\text{spp}} + \mu \mathbf{H}^*_{\text{spp}} \times \mathbf{H}_{\text{spp}})/2\omega, \tag{3}$$

as can be derived from the spin formula in Ref. 28 with appropriate substitutions for time-harmonic fields. We show a three-dimensional view of the vectors of this experimental spin field in

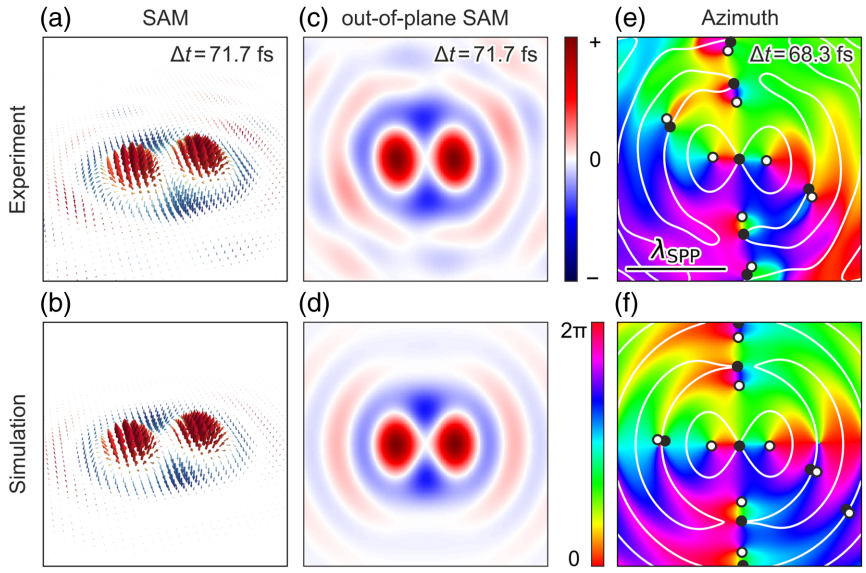

Fig. 3 A comparison between experiment and simulation for the spin vectors of the SPP meron pair. (a), (b) The spin vectors demonstrating the presence of the meron pair. The time evolution of the experimentally determined spin vectors is shown in Video 3. (c), (d) The out-of-plane spin components s_z where the color encodes the spin direction. The spin is zero in the white regions that locate L lines. (e), (f) The directions of in-plane components of the spin vectors are represented by the color hue. The time evolution of the experimentally determined azimuth is shown in Video 4. The white lines are the L lines where the out-of-plane spin is $s_z = 0$. The points where the in-plane vectors are zero (the zeroes of the field) are marked with dots, where white corresponds to zeroes with vorticity $v = +1$ and black for zeroes with vorticity $v = -1$. (Video 3, M4V, 5.8 MB [URL: https://doi.org/10.1117/1.AP.6.6.066007.s3]; Video 4, M4V, 2.1 MB [URL: https://doi.org/10.1117/1.AP.6.6.066007.s4].)

Fig. 3(a), which reveals two vortex quasi-particles, with spin vectors directed out of the plane, embedded in a region of weak downward directed spins.

As we show below, each of these features has the local topology of a meron, and thus, this quasi-particle corresponds to a "meron pair." From the measured time sequence of the SPP spin field, we find that the quasi-particle is stable for at least 23 fs, as shown in Video 3, a value close to the overlap time of the pulsed SPP waves arriving from opposite sides of the Archimedean spiral. This stability arises despite the complex time and space variations of the underlying electromagnetic fields. The experimentally determined meron pair shows excellent agreement with the theoretical model [Fig. 3(b)] based on a simulation of the SPP electric fields.[29] Remarkably, the measured spin distribution of this SPP meron pair also shows qualitative agreement with simulated magnetic meron pairs expected in thin films[30] but which have not yet been measured to such fine detail in magnetic systems. The out-of-plane spin components s_z are shown for both experiment and simulation in Figs. 3(c) and 3(d). The white regions in these color plots highlight the lines along which the out-of-plane spin component is zero, $s_z = 0$. These are the L lines where the in-plane electric fields are linearly polarized and show no in-plane rotation.

An important topological feature of our measured vector field arises where the in-plane vectors are zero ($s_x = s_y = 0$). Such "zeroes" of the in-plane field come in two types, one being a C point[31] where the spin field is oriented completely out of the plane ($s_z \neq 0$), and the other being an amplitude vortex[20] where the complete spin falls to zero ($s_x = s_y = s_z = 0$). Both C points and amplitude vortices of the spin field can be assigned a vorticity $v = \pm 1$ according to the direction of rotation of the vectors on a path about them, as depicted in Fig. 1(a). This property is shown by the change in the hue on traversing a path about a zero point, such as from blue to green or blue to red in Fig. 3(e) for the experimentally determined spin fields and in Fig. 3(f) for the numerical simulation. The zeroes of the field are highlighted by white dots ($v = +1$) and black dots ($v = -1$) in Figs. 3(e) and 3(f). It is clear that each of the merons in Fig. 3(a) is associated with a C point with a vorticity $v = 1$ and a polarity $p = 1/2$ because $s_z > 0$; therefore, each has a Chern number of $C = p \cdot v = 1/2$ or a total of $C = 1$, as expected. Between the two merons, the spin magnitude goes to zero [cf. Figs. 3(a) and 3(b)], which corresponds to an amplitude vortex mid-way between the C points. This amplitude vortex has a vorticity of $v = -1$, and its presence is required by topology, as will be discussed below.

The vorticities associated with the zeroes of the in-plane spin field depicted in Figs. 3(e) and 3(f) have a fundamental connection to topology such that vector fields with different vorticity are nonhomotopic, i.e., they have a different topology.[22] The vorticity, when calculated around any zero, is also known as the Poincaré index. This index is positive or negative according to the direction of rotation of the field about the zero, exactly as shown for the vorticities in Fig. 1(a). Poincaré proved that the sum of the vorticities of a vector field is equal to the Euler characteristic χ, which is a fundamental topological invariant.

In our experiment, the SPPs created at each point on the Archimedean spiral have in-plane spin vectors parallel to the

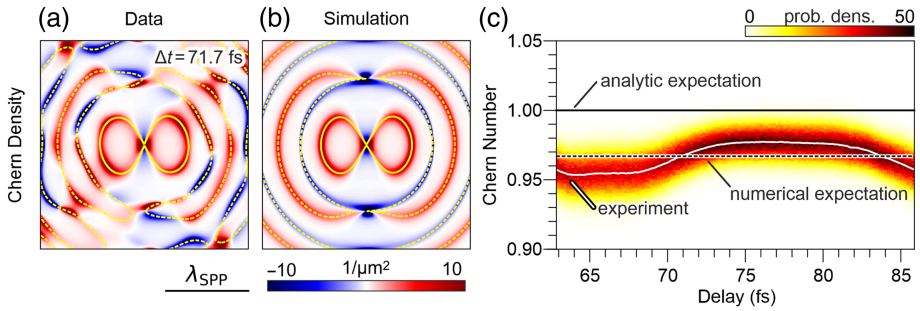

Fig. 4 Topology of the SPP meron pair. (a) The experimental Chern density [kernel of Eq. (1)]. The time evolution of the experimental Chern density is shown in Video 5. (b) The expected Chern density based on a numerical simulation of the SPP's electric fields and their subsequent spin fields. The *L* lines are marked in yellow. (c) The Chern number within the marked solid *L* line in panels (a) and (b) as a function of pump–probe delay. The experimental Chern number is shown as a white line; the result from a numerical simulation is shown as a dashed line, and the theoretical value of $C = 1$ is shown as a solid black line. The colored background represents the data reliability, based on a Monte-Carlo-based error propagation assuming a 10 nm spatial resolution. (Video 5, M4V, 2.33 MB [URL: https://doi.org/10.1117/1.AP.6.6.066007.s5].)

tangents of the grooves and therefore, on propagating over the surface, have the topology of a disk for which the Euler characteristic is $\chi = 1$. As shown in Figs. 3(e) and 3(f), most of the zeroes come in pairs of opposite index, which therefore cancel. Because the meron pair involves two zeroes, each with vorticity $v = +1$, it is a topological necessity that there must be another zero with vorticity $v = -1$ such that the sum of the vorticities equals the Euler characteristic, $\chi = 1$. This is the origin of the amplitude vortex that lies between the two *C* points of the meron pair. Based on the Euler characteristic, we expect all other zeroes to appear in pairs of opposite indices to maintain $\chi = 1$. If an additional isolated vortex exists within the imaged field of view, a corresponding vortex with opposite vorticity must exist outside the field of view to fulfill the Poincaré–Hopf theorem. For the infinitely extending case of the meron spin fields, there is an infinite number of zeroes from *C* points and amplitude vortices whose indices (except one) cancel pairwise. The measured out-of-plane components are essential for determining the polarity to distinguish between true spin vortices (*C* points) and amplitude vortices. This highlights the importance of using polarimetric PEEM to measure the complete spin vector direction when using $C = p \cdot v$ to determine the Chern number: the in-plane components alone are insufficient to characterize the spin topology.

The relationship between vorticity and the Euler characteristic implies a vortex conservation law in the two-dimensional vector field: vortices can only be created or annihilated in pairs with vortices of opposite sign[21,22] such that the Euler characteristic remains constant. Because this is a constraint on the topology, the Poincaré sum becomes a global constraint on the in-plane components of the vector spin fields that impact the local properties of their zeroes. The topological connection between local and global properties arises in other fields, as with defects in crystals,[32] for example, screw dislocations where the local line defect represents a topological charge that impacts the crystal structure at large distances. In our time-dependent measures of spin texture, we observe such vortex pair creation and annihilation experimentally, which we show in Video 4.

From the measured spatiotemporal properties of the SPP spin field, we calculate the Chern density, which is the kernel of the integral in Eq. (1). The Chern density obtained from experimental spin data at a delay time of $\Delta t = 71.7$ fs is shown in Fig. 4(a), with that calculated from a simulation shown for comparison in Fig. 4(b). The temporal dependence of the Chern density is shown in Video 5. The Chern number is the integral of the Chern density over a suitable region of the SPP field. However, to correctly measure the local topology, we need to limit the integral to the area close to the meron pair. The boundary of the integral is chosen as the *L* line surrounding the spin feature,[14] which is defined by the points where $s_z = 0$ because the in-plane electric field vectors on this line are perfectly linearly polarized. The *L* lines in the measured data are marked in yellow in Fig. 4(a). With the experimentally determined SPP spin in Eq. (1), we obtain the time-dependent Chern number shown in Fig. 4(c). The experimental data gives slightly varying numbers that strongly depend on the chosen *L* line integration contour. Adding noise to the positioning of the contour in a Monte-Carlo-based error propagation, using the electron-optical resolution of the microscope of 10 nm, results in experimental Chern numbers within the color-coded probability density in the background in Fig. 4(c). The temporal dependence of the Chern number shows that the meron pair remains topologically stable for the period of time where the SPP waves from the boundary overlap and interfere at the center of the sample.

We note that the theoretical expectation is a Chern number of 1 for the meron pair because each meron contributes a Chern number of 1/2. The Chern number obtained from a temporal average of the experimental data is $C = 0.97$. This number is smaller than $C = 1$ due to the infinitely small central amplitude vortex and the finite pixelation of the data. How the Chern number depends on the resolution and pixelation is discussed in detail in Supplementary Material (Note 6). The dependence of the Chern number on the resolution emphasizes the importance of gathering high-resolution spatial measurements of the SPP field to extract the underlying topology and proper Chern numbers. A pixelation of 12 nm, which corresponds to the pixelation by the electron detector, is expected to yield a Chern number of $C = 0.97$ [cf. the numerical expectation in Fig. 4(c)].

4 Conclusion and Outlook

In our analysis, we have identified regions in the SPP spin field associated with *C* points and *L* lines and unambiguously identified a meron pair. It is worth remarking that these are equivalent to the topology of a landscape as Maxwell also investigated,[33] where the contour lines and their relationship to points representing maxima (hills) or minima (dales) appear, respectively, such as the *L* lines and *C* points here. The determination of the SPP spin topology was only possible using our polarimetric PEEM method, which enables the measurement of the three-dimensional SPP vector fields and their evolution in time. The topology of these SPP vector fields is generally hidden in the static field distributions obtained from interferometric optical near-field measurements, and the presence of amplitude vortices can further complicate the analysis.

The time and space resolution that we obtain provides opportunities for studying other complex vector wave interference phenomena dictated by an underlying topology, such as wave patterns associated with two-dimensional quasi-crystals.[34] Although we have demonstrated polarimetric PEEM with long-range surface plasmons, the method is equally well suited to studying short-range surface plasmons. These short-range SPPs have potential as highly compact localized field sources with wavelengths an order of magnitude smaller than the excitations in free space.[35–37] Such fields can be intense, yielding possibilities for highly localized excitation and interactions with potential applications in structured light illumination and microscopy, as well as in complex light-field–matter interaction. Topology then becomes an important tool for controlling near fields at the nanoscale because topological protection can help stabilize the field geometries.[38]

Disclosures

The authors declare no competing interest.

Code and Data Availability

The data used for the analysis will be made available upon reasonable request.

Author Contributions

P.D., A.N., D.J., F.MzH., and A.R. performed the time-resolved PEEM experiments. B.F. and T.M. prepared the samples. P.D., D.J., F.MzH., and H.G. conceived the experiment. P.D., A.N., D.J., T.D., and F.MzH. analyzed the data. T.D., D.J., P.D., F.MzH., and H.G. wrote the manuscript with contributions from all authors.

Acknowledgments

The authors acknowledge support from the ERC (Complexplas, 3DPrintedoptics), DFG (SPP1391 "Ultrafast Nanooptics," CRC 1242 "Non-Equilibrium Dynamics of Condensed Matter in the Time Domain" Grant Nos. 278162697-SFB 1242 and GRK2642 "Photonic Quantum Engineers"), BMBF (Printoptics), BW Stiftung (Spitzenforschung, Opterial), Carl-Zeiss Stiftung. T.J.D. acknowledges support from the MPI Guest Professorship Program and from the DFG (Grant No. GRK2642 "Photonic Quantum Engineers") for a Mercator Fellowship. We acknowledge fruitful discussions about topology with Karin Everschor-Sitte and David Paganin for alerting us to Maxwell's paper on topology.

References

1. J. E. Avron, D. Osadchy, and R. Seiler, "A topological look at the quantum hall effect," *Phys. Today* **56**(8), 38–42 (2003).
2. N. Nagaosa and Y. Tokura, "Topological properties and dynamics of magnetic skyrmions," *Nat. Nanotechnol.* **8**(12), 899–911 (2013).
3. K. Everschor-Sitte et al., "Perspective: magnetic skyrmions—overview of recent progress in an active research field," *J. Appl. Phys.* **124**(24), 240901 (2018).
4. N. Romming et al., "Writing and deleting single magnetic skyrmions," *Science* **341**(6146), 636–639 (2013).
5. R. Knapman et al., "Current-induced h-shaped-skyrmion creation and their dynamics in the helical phase," *J. Phys. D: Appl. Phys.* **54**(40), 404003 (2021).
6. M. Ezawa, "Compact merons and skyrmions in thin chiral magnetic films," *Phys. Rev. B* **83**(10), 100408 (2011).
7. N. Gao et al., "Creation and annihilation of topological meron pairs in in-plane magnetized films," *Nat. Commun.* **10**(1), 5603 (2019).
8. T. Shinjo et al., "Magnetic vortex core observation in circular dots of permalloy," *Science* **289**(5481), 930–932 (2000).
9. C. Phatak, A. Petford-Long, and O. Heinonen, "Direct observation of unconventional topological spin structure in coupled magnetic discs," *Phys. Rev. Lett.* **108**(6), 067205 (2012).
10. X. Yu et al., "Transformation between meron and skyrmion topological spin textures in a chiral magnet," *Nature* **564**(7734), 95–98 (2018).
11. Y. Shen et al., "Optical skyrmions and other topological quasiparticles of light," *Nat. Photonics* **18**(1), 15–25 (2024).
12. M. Król et al., "Observation of second-order meron polarization textures in optical microcavities," *Optica* **8**(2), 255–261 (2021).
13. L. Xiong et al., "Polaritonic vortices with a half-integer charge," *Nano Lett.* **21**(21), 9256–9261 (2021).
14. Y. Dai et al., "Plasmonic topological quasiparticle on the nanometre and femtosecond scales," *Nature* **588**(7839), 616–619 (2020).
15. A. Ghosh et al., "A topological lattice of plasmonic merons," *Appl. Phys. Rev.* **8**(4), 041413 (2021).
16. D. Janoschka et al., "Implementation and operation of a fiber-coupled CMOS detector in a low energy electron microscope," *Ultramicroscopy* **221**, 113180 (2021).
17. P. Kahl et al., "Normal-incidence photoemission electron microscopy (NI-PEEM) for imaging surface plasmon polaritons," *Plasmonics* **9**(6), 1401–1407 (2014).
18. B. Radha et al., "Movable Au microplates as fluorescence enhancing substrates for live cells," *Nano Res.* **3**(10), 738–747 (2010).
19. B. Göbel, I. Mertig, and O. A. Tretiakov, "Beyond skyrmions: review and perspectives of alternative magnetic quasiparticles," *Phys. Rep.* **895**(0), 1–28 (2021).
20. T. Fösel, V. Peano, and F. Marquardt, "L lines, C points and Chern numbers: understanding band structure topology using polarization fields," *New J. Phys.* **19**(11), 115013 (2017).
21. M. R. Dennis, K. O'Holleran, and M. J. Padgett, "Chapter 5 singular optics: optical vortices and polarization singularities," *Prog. Opt.* **53**(0), 293–363 (2009).
22. D. S. Simon, *Tying Light in Knots*, pp. 2053–2571, Morgan & Claypool Publishers (2018).
23. J. Nye and J. Hajnal, "The wave structure of monochromatic electromagnetic radiation," *Proc. R. Soc. Lond. A* **409**(1836), 21–36 (1987).
24. M. Berry and M. Dennis, "Polarisation singularities in isotropic random vector waves," *Proc. R. Soc. Lond. A* **457**, 141–155 (2001).
25. T. Davis et al., "Ultrafast vector imaging of plasmonic skyrmion dynamics with deep subwavelength resolution," *Science* **368**(6489), eaba6415 (2020).
26. D. Podbiel et al., "Imaging the nonlinear plasmoemission dynamics of electrons from strong plasmonic fields," *Nano Lett.* **17**(11), 6569–6574 (2017).

27. P. Dreher et al., "Momentum space separation of quantum path interferences between photons and surface plasmon polaritons in nonlinear photoemission microscopy," *Nanophotonics* **13**(9), 1593–1602 (2024).
28. S. M. Barnett, "Rotation of electromagnetic fields and the nature of optical angular momentum," *J. Mod. Opt.* **57**(14), 1339–1343 (2010).
29. T. Davis et al., "Subfemtosecond and nanometer plasmon dynamics with photoelectron microscopy: theory and efficient simulations," *ACS Photonics* **4**(10), 2461–2469 (2017).
30. X. Lu et al., "Meron-like topological spin defects in monolayer $CrCl_3$," *Nat. Commun.* **11**(1), 4724 (2020).
31. J. Nye, "Lines of circular polarization in electromagnetic wave fields," *Proc. R. Soc. Lond. A* **389**(1797), 279–290 (1983).
32. N. Mermin, "The topological theory of defects in ordered media," *Rev. Mod. Phys.* **51**(3), 591–648 (1979).
33. J. C. Maxwell, "L. On hills and dales," *Lond. Edinburgh Dublin Philos. Mag. J. Sci.* **40**(269), 421–427 (1870).
34. Z. Vardeny, A. Nahata, and A. Agrawal, "Optics of photonic quasicrystals," *Nat. Photonics* **7**(3), 177–187 (2013).
35. L. Du et al., "Deep-subwavelength features of photonic skyrmions in a confined electromagnetic field with orbital angular momentum," *Nat. Phys.* **15**(7), 650–654 (2019).
36. B. Frank et al., "Short-range surface plasmonics: localized electron emission dynamics from a 60-nm spot on an atomically flat single-crystalline gold surface," *Sci. Adv.* **3**(7), e1700721 (2017).
37. Y. Shen et al., "Supertoroidal light pulses as electromagnetic skyrmions propagating in free space," *Nat. Commun.* **12**(1), 5891 (2021).
38. H. Xue, Y. Yang, and B. Zhang, "Topological valley photonics: physics and device applications," *Adv. Photonics Res.* **2**(8), 2100013 (2021).
39. M. U. Wehner, M. H. Ulm, and M. Wegener, "Scanning interferometer stabilized by use of pancharatnam's phase," *Opt. Lett.* **22**, 1455–1457 (1997).
40. F. J. Meyer zu Heringdorf et al., "Spatio-temporal imaging of surface plasmon polaritons in two photon photoemission microscopy," *Proc. SPIE* **9921**, 992110 (2016).
41. J. S. Li et al., "An advanced phase retrieval algorithm in *N*-step phase-shifting interferometry with unknown phase shifts," *Sci. Rep.* **7**(1), 44307 (2017).
42. A. Kubo, N. Pontius, and H. Petek, "Femtosecond microscopy of surface plasmon polariton wave packet evolution at the silver/vacuum interface," *Nano Lett.* **7**(2), 470–475 (2007).

Pascal Dreher is a PhD candidate in the faculty of physics at the University of Duisburg-Essen, where he is currently pursuing his doctoral studies. He holds a Bachelor of Science degree (2016) and a Master of Science degree (2018) in physics from the same institution. His research interests lie in the field of nanooptics and plasmonics, with a focus on surface plasmon polariton dynamics and their interactions with matter.

Alexander Neuhaus is a doctoral student in the faculty of physics at the University of Duisburg-Essen, where he is working towards his PhD. He previously earned a Bachelor of Science degree in physics in 2020 and a Master of Science degree in physics in 2022, both from the University of Duisburg-Essen. His research focuses on nanooptics and plasmonics, with a particular emphasis on the dynamics of surface plasmon polaritons and their interactions with matter.

David Janoschka is a physicist with a PhD from the University of Duisburg-Essen, earned in 2023. His research focused on the polarimetric PEEM project, advancing the understanding of topology in plasmonic systems. He has now transitioned from academia to industry, applying his analytical skills to the design of Germany's future energy infrastructure.

Alexandra Roedl is a recent Master of Science graduate in physics from the University of Duisburg-Essen, Germany. She completed her bachelor's degree in 2020 and her master's degree in 2023. During her master's thesis, she worked on the time-resolved PEEM project, exploring topology of plasmonic patterns. She has now transitioned into a career in data science, applying her analytical skills and knowledge of physics to drive insights and innovation.

Tim Colin Meiler received his BSc degree from University of Stuttgart in 2021 and is a PhD student at Nanyang Technological University, Singapore. He is currently researching novel materials in nanophotonics to miniaturize tuneable lasers and spatial light modulators driven by microheaters. His research interests include optical skyrmions, phase change materials, nano-optics, and metasurfaces.

Bettina Frank is a permanent post-doctoral researcher at the University of Stuttgart in Germany. She received her diploma and PhD in physics from the University of Stuttgart in 2010 and 2016, respectively. Since then, her research interests focus mainly on various synthesis and characterization methods of single crystalline gold platelets, nanofabrication, plasmonics, topology, and various near-field microscopy technologies.

Timothy J. Davis is a guest professor in the 4th Physics Institute at the University of Stuttgart, Germany, a visiting professor at the University of Duisbug-Essen, Germany and an honorary research fellow in the School of Physics, University of Melbourne, Australia. He holds a PhD in experimental physics and was a senior principal research scientist at CSIRO Australia until 2015. His research interests include electromagnetic wave phenomena and nanooptics.

Harald Giessen is a full professor and holds the Chair for Ultrafast Nanooptics in the Department of Physics at the University of Stuttgart. He is also co-chair of the Stuttgart Center of Photonics Engineering, SCoPE. He received his MS and PhD in optical sciences from the University of Arizona in 1995. After a postdoc at the MPI for Solid State Research in Stuttgart he moved to Marburg as assistant professor. From 2001 to 2004, he was an associate professor at the University of Bonn. His research interest is ultrafast nanooptics.

Frank Meyer zu Heringdorf is a professor of physics at the University of Duisburg-Essen and scientific director of the Interdisciplinary Center of Analytics on the Nanoscale (ICAN). After learning low-energy electron microscopy during a postdoctoral stay as a Feodor Lynen Fellow at the IBM Research Laboratory in Yorktown Heights, he established a laboratory for ultrafast photoemission microscopy in Duisburg. His research interests include surface plasmon polaritons and their coupling to the electron system, as well as the growth of 2D materials.